Received 25 July 2024; accepted 19 August 2024. Date of publication 26 August 2024; date of current version 12 September 2024.

*Digital Object Identifier 10.1109/OJCOMS.2024.3450089*

# Geometrical Features Based-mmWave UAV Path Loss Prediction Using Machine Learning for 5G and Beyond

**SAJJAD HUSSAIN[1], SYED FARAZ NAEEM BACHA[1], ADNAN AHMAD CHEEMA[2] (Member, IEEE), BERK CANBERK[3,4] (Senior Member, IEEE), AND TRUNG Q. DUONG[5,6] (Fellow, IEEE)**

[1]School of Electrical Engineering and Computer Science, National University of Sciences and Technology, Islamabad 44000, Pakistan

[2]School of Engineering, Ulster University, BT15 1AP Belfast, U.K.

[3]Department of Artificial Intelligence and Data Engineering, Istanbul Technical University, 34467 Istanbul, Türkiye

[4]School of Computing, Engineering and The Build Environment, Edinburgh Napier University, EH11 4BN Edinburgh, U.K.

[5]School of Electronics, Electrical Engineering and Computer Science, Queen's University, BT7 1NN Belfast, U.K.

[6]Faculty of Engineering and Applied Science, Memorial University of Newfoundland, St. John's, NL A1C 5S7, Canada

CORRESPONDING AUTHOR: T. Q. DUONG (e-mail: tduong@mun.ca)

The work of Berk Canberk was supported by the Scientific and Technological Research Council of Turkey (TUBITAK) 1515 Frontier Research and Development Laboratories Support Program for BTS Advanced AI Hub: BTS Autonomous Networks and Data Innovation Lab. Project 5239903. The work of Trung Q. Duong was supported in part by the Canada Excellence Research Chair (CERC) Program under Grant CERC-2022-00109.

**ABSTRACT** Unmanned aerial vehicles (UAVs) are envisioned to play a pivotal role in modern telecommunication and wireless sensor networks, offering unparalleled flexibility and mobility for communication and data collection in diverse environments. This paper presents a comprehensive investigation into the performance of supervised machine learning (ML) models for path loss (PL) prediction in UAV-assisted millimeter-wave (mmWave) radio networks. Leveraging a unique set of interpretable geometrical features, six distinct ML models–linear regression (LR), support vector regressor (SVR), K nearest neighbors (KNN), random forest (RF), extreme gradient boosting (XGBoost), and deep neural network (DNN)–are rigorously evaluated using a massive dataset generated from extensive ray-tracing (RT) simulations in a typical urban environment. Our results demonstrate that the RF algorithm outperforms other models showcasing superior predictive performance for the test dataset with a root mean square error (RMSE) of 2.38 dB. The proposed ML models demonstrate superior accuracy compared to 3GPP and ITU-R models for mmWave radio networks. This study thoroughly investigates the adaptability of these models to unseen environments and examines the feasibility of training them with sparse datasets to improve accuracy. The reduction in computation time achieved by using ML models instead of extensive RT computations for sparse training datasets is evaluated, and an efficient algorithm for training such models is proposed. Additionally, the sensitivity of ML models to noisy input features is analyzed. We also assess the importance of geometrical features and the impact of sequentially increasing the number of these features on model performance. The results emphasize the significance of the proposed geometrical features and demonstrate the potential of ML models to provide computationally efficient and relatively accurate PL predictions in diverse urban environments.

**INDEX TERMS** UAVs, millimeter-wave (mmWave), 5G, path loss (PL), ray tracing, and machine learning.

## I. INTRODUCTION

UNMANNED aerial vehicle (UAV) communication is becoming a critical part of achieving the expected benchmark performance of future wireless networks and to increase the coverage [1], [2], [3]. UAV communications provide improved coverage and quality of service due to having a high probability of line of sight (LOS) links [4], [5], [6], [7]. Due to their 3D mobility, such UAV communications can bring a rapid transformation in a wide spectrum of use

cases in telecommunication and wireless sensor networks in smart cities, precision agriculture, public safety, disaster management, smart manufacturing, and health [8], [9], [10], [11], [12], [13], [14]. It is projected that UAV-based services and applications can attract USD 38.3 billion by 2027 [15]. Despite recent advancements, there remain significant research challenges to maximize the potential of UAV communications, necessitating further advancements in channel modeling, mobility management, integration into terrestrial and non-terrestrial networks, and leveraging ML to optimize these solutions. Recently, millimeter-wave (mmWave), providing high data rate due to availability of large bandwidth, reducing antenna size to realize massive MIMO and minimizing interference using concepts of beamforming, has been considered to be integrated into UAV for performance enhancement [16].

Channel modeling plays an important role in establishing a functional wireless network which is optimized by considering the characteristics of the environment and associated channel parameters [17]. Traditional radio channel modeling techniques including field measurements [18], deterministic models [19], and stochastic models [20] suffer limitations in accurate UAV channel prediction. The ML based models can overcome the limitations of field measurement (site-specific), deterministic models (high computational complexity) and stochastic models (lower accuracy). The existing literature presents various approaches for PL prediction and signal strength estimation in UAV-assisted mmWave communication channels [21], [22], [23], [24], [25], [26], [27], [28], [29], [30].

Path delay, reflection angle, and carrier frequency were utilized as input features in [21] to train an artificial neural network (ANN) model for accurate PL prediction in air-to-ground (A2G) channels. Initially, a massive ray-tracing (RT) dataset was employed, which was subsequently fine-tuned with measured data. Similarly, PL under both line-of-sight (LOS) and non-line-of-sight (NLOS) conditions were predicted in [22] using a back propagation neural network (BPNN). This was achieved using simulated RT data, with path delay and reflection angle as the sole input features. Geographical features, including distance, heights, terrain types, and shadowing buildings, were leveraged in [23] using a multi-layer perception (MLP) to forecast signal strength coverage across various cities based on measured data. RF and KNN was employed in [24] to predict PL and delay spread in A2G mmWave channels. Their approach involved utilizing the XY coordinates of UAVs, propagation distance, shadowing buildings, and elevation angle as input features. These features were selected through an iterative feature selection scheme, enabling the training of models using RT datasets. In a related work [25], an ML framework was proposed, leveraging an extensive list of sixteen features extracted from raw network data, including site topology and various geographical datasets such as digital terrain, digital height, and digital land use maps, alongside user equipment (UE) measurement traces. A range of supervised regression models were evaluated for predictive accuracy, generalization performance, and computational efficiency. In a few recent studies [26], [27], [28], [29], the stacked generalization of ensemble models is investigated, where diverse base learners were combined to produce an optimized meta learner for enhanced performance. In [26], the structure of base learners like XGBoost, Light gradient boosting machine (LightGBM), and categorical boosting (Catboost) was fine-tuned to achieve superior predictive accuracy using the whale optimization algorithm. In [27], building height parameters were extracted using image processing techniques, enriching the dataset for PL prediction against measured data using an ensemble model comprising SVR, RF, ANN, XGBoost, LightGBM, KNN, and adaptive boosting (AdaBoost), followed by a meta LR model. Similarly, in [29], SVR, gaussian process (GP), ANN, least square boosting (LSBoost), and bagging base learners were stacked to yield a weighted average meta model predicting received signal strength using fundamental features such as height, distance, and XY coordinates against measured data.

While there has been considerable research on ML-based PL prediction models in recent years, much of the reported work has relied either on complex features derived from field measurements that can be challenging to obtain, or on simpler features like distance, heights, coordinates, and frequency that make these models similar to traditional PL models. However, in contrast to these approaches, our proposed model incorporates a unique set of *interpretable geometrical features*, that account for site-specific details. These features can be easily computed without the need for computationally intensive RT algorithms, thus enhancing the adaptability of ML models to a wider range of urban environments.

The contributions of this research work are summarized as follows:

- A comprehensive performance evaluation of six distinct supervised ML models, including LR, SVR, KNN, RF, XGBoost, and DNN is carried out. These models are trained using a unique set of geometrical features on a dataset generated through RT simulations in a typical urban environment. The results show that the mean RMSE of all the models except LR is below 3 dB using the proposed geometrical features.The proposed models have also shown better accuracy than 3GPP and ITU-R models.
- The study evaluates the trained models' generalization capabilities in new environments and evaluates the increase in accuracy and reduction in computation times for training with sparse datasets.
- We assess the impact of noisy input features and the significance of geometrical features on model performance, including the effect of incrementally adding these features.

The subsequent sections of this paper are outlined as follows: Section II details the methodology for generating

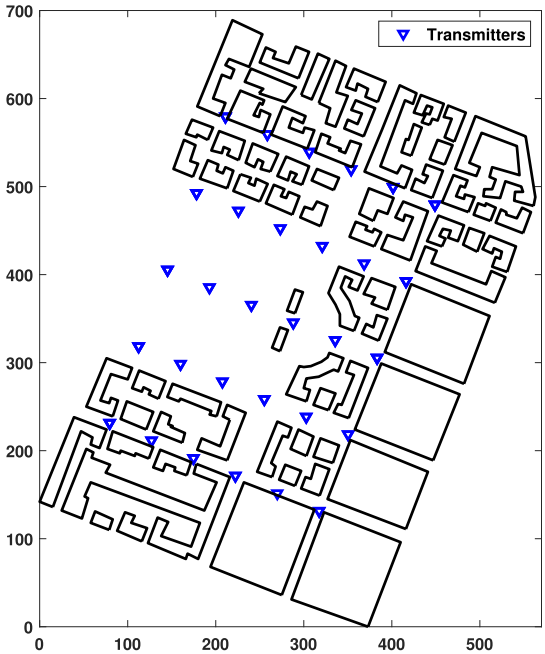


FIGURE 1. Top view of the simulated environment used for dataset generation.

a comprehensive dataset and identifying unique geometrical features crucial for PL prediction. In Section III, we summarize the models developed through an extensive hyper-parameter tuning process. Section IV provides a thorough evaluation of the supervised ML models' performance on both the test dataset and in generalizing to unseen environments. Additionally, we introduce an efficient algorithm tailored to enhance predictive performance using sparse training data. An analysis of the importance of geometrical features and their impact on model performance with varying feature sets is also included. Finally, Section V presents the conclusion.

## II. DATASET GENERATION AND FEATURE ENGINEERING

### A. SIMULATION SETUP AND DATASET GENERATION

In order to train the ML models, a large dataset is required. The dataset used in this paper is generated using an in-house RT model that has been validated in previous works [31], [32], [33]. The simulated scenario consists of 67 buildings within a 400m x 600m area and is taken from Munich city as shown in Fig. 1. This environment is labeled as Munich-1 for future reference in this paper. The average building height in the simulated environment is about 20m. RT simulations are performed to compute the received power through direct LOS, first-order specular wall reflection, and ground-reflection rays between the transmitter and receiver. A half-wave dipole transmitter antenna with 30 dBm output power at 28 GHz carrier frequency is used. The RT model also incorporates the diffused scattering contributions at the receiver due to first-order wall reflections. The single lobe directive scattering model, as proposed in [34] is used to compute the Diffuse scattered fields. The simulations are performed for a total of 36 different locations of the transmitter, each at three different altitudes of 25m, 35m, and 45m. The valid rays are computed between each transmitter to a grid of $6,074$ receiver points distributed across the environment at a resolution of 5m x 5m. It is assumed that the vector database of the buildings, UAV position, and receiver grid locations are known a priori. The height of the receiver points is 1.5m. Building walls are modeled as solid concrete. The buildings are oriented according to their real-world coordinates and are not intentionally rotated. Only the receiver points within the rectangular area defined by the perimeter of the buildings at the border of the environment are considered, while the open areas outside this perimeter are discarded. Table 1 summarizes the simulation parameters used for the RT model to generate the dataset.

TABLE 1. RT model simulation parameters for dataset generation.

| Parameters | Description |
|---|---|
| Environment | Urban outdoor micro-cellular |
| Average building height | 19.68 m |
| Building material | Concrete |
| Wall permittivity ($\epsilon_r$) | 5.31 |
| Simulation frequency | 28 GHz |
| Transmitter Power | 30 dBm |
| Antenna type | Dipole Antenna |
| UAV height range | 25, 35, and 45 meters |
| Receiver Grid | $6,074$ receivers at 5 m x 5 m resolution |
| Receiver height | 1.5 m |
| Reflection | First order specular & ground reflection |
| Scattering model | Directive scattering [34] |

### B. GEOMETRICAL FEATURES FOR MODELS TRAINING

The RT model computes PL for 250, 514 distinct transmitter-receiver pairs. Simultaneously, the RT model computes a distinctive set of geometrical features for each transmitter-receiver pair in the dataset, as shown in Fig. 2. These features, crucial for subsequent analyses, are comprehensively outlined in Table 2. In this study, UAV does not measure these features as these are computed using the geometrical data of buildings vector database, UAV position and receivers location.

The foremost critical feature is the direct three-dimensional (3D) distance between the transmitter and the receiver. The remaining features can be broadly categorized into three sub-groups. The features related to visibility account for the reflection rays arriving at the given receiver location. This category includes the count of

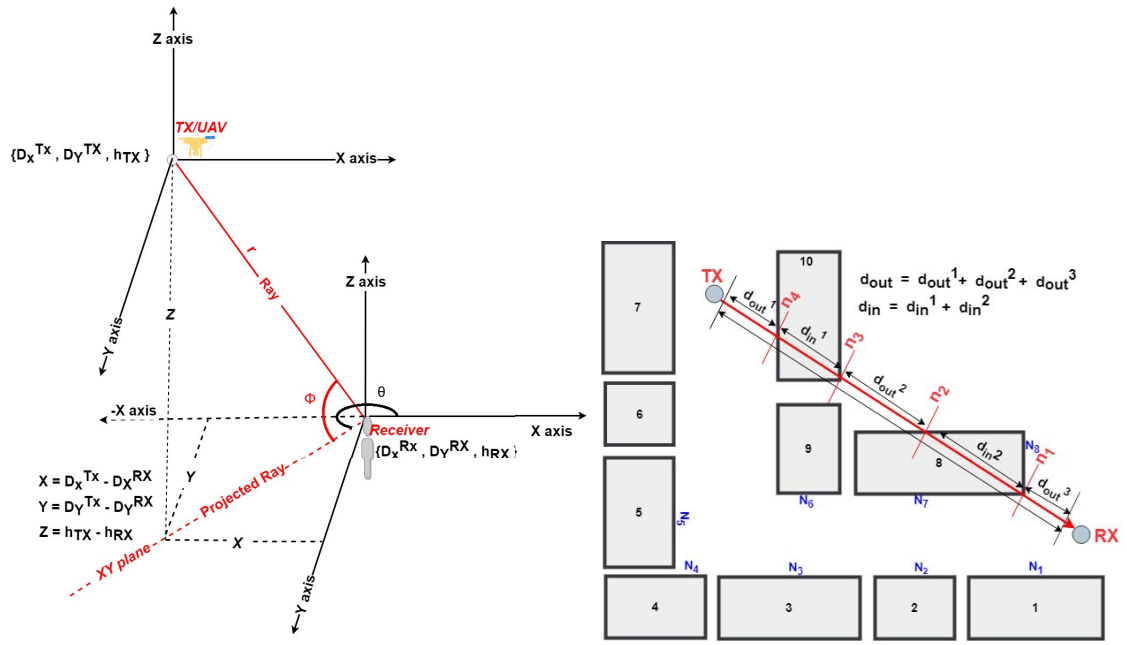


FIGURE 2. Computation of geometrical features including (a) 3D distance (r), UAV height ($h_{TX}$), angles ($\theta$, $\phi$), and (b) visibility and shadowing features.

TABLE 2. A detailed description of geometrical features derived from the propagation environment.

| *Feature* | Notation | Description |
|---|---|---|
| 3d_distance | r | 3D distance between the UAV and receiver (RX). |
| no_visible_walls | $N_{wall}$ | Number of walls that are partially or completely visible to the receiver, meaning there are no obstructions between the receiver and any part of these walls. |
| min_distance_to_walls | $D_{min}$ | Distance to the nearest visible wall from the receiver. |
| avg_distance_to_walls | $D_{avg}$ | The average distance to all visible walls from the receiver and is given by the sum of distances to all the visible walls divided by the number of visible walls. |
| Transmitter_ZZ | $h_{TX}$ | Height of UAV |
| walls_pen | n | The number of building walls intersected by the direct line connecting UAV and RX in the XY plane. |
| indoor_distance | $d_{in}$ | Distance traveled inside the buildings by the direct line joining UAV and RX in the XY plane. |
| outdoor_distance | $d_{out}$ | The length of the direct line joining UAV and RX in the XY plane that does not go through the buildings and is outside. |
| min_wall_height | $H_{min}$ | The minimum height of all the building walls intersected by the direct line joining UAV and RX in the XY plane. |
| max_wall_height | $H_{max}$ | The maximum height of all the building walls intersected by the direct line joining UAV and RX in the XY plane. |
| avg_wall_height | $H_{avg}$ | The average height of all the building walls intersected by the direct line joining UAV and RX in the XY plane. |
| Theta | $\theta$ | The angle between the line connecting UAV and RX in the XY plane with the positive X-axis. |
| Phi | $\phi$ | The elevation angle between RX and UAV with respect to the XY-plane. |

visible building walls at the given receiver location, along with metrics such as the minimum and average distances between a receiver and the visible walls. Additionally, it accounts for the transmitter's height, a critical factor influencing the number of building walls directly visible to the transmitter. The second category focuses on features

**TABLE 3.** Summary of hyperparameters for different ML models.

| Model | Parameter 1 | Parameter 2 | Parameter 3 | Parameter 4 | Parameter 5 |
|---|---|---|---|---|---|
| **LR** | - | - | - | - | - |
| **KNN** | n_neighbors = 4 | - | - | - | - |
| **RF** | n_estimators = 1000 | max_depth = 50 | min_samples_leaf = 2 | - | - |
| **XGBoost** | n_estimators = 300 | max_depth = 10 | learning_rate = 0.5 | subsample = 1 | colsample_bytree = 1 |
| **SVR** | Kernel = RBF | C = 30 | Gamma ($\gamma$) = 1.2 | Epsilon($\epsilon$) = 2 | - |
| **DNN** | Layers = 3 | Nodes = 250 | Activation = $tanh$ | Optimizer = Adam | Learning rate = 0.001 |

associated with shadowing caused by buildings obstructing the direct path between the transmitter and receiver. These features include the count of building walls situated in the horizontal plane between the transmitter and receiver, the distances covered both inside and outside the shadowed buildings along the direct line connecting the transmitter and receiver in the horizontal plane, and metrics related to the minimum, maximum, and average heights of the shadowing buildings. Fig. 2(b) shows an example of the computation of shadowing features as there are 4 walls ($n_1$ to $n_4$) between the transmitter and receiver. Likewise, the total indoor and outdoor shadowed region is computed as $d_{in}$ and $d_{out}$ respectively. The example also shows the visibility features as there are 8 walls ($N_1$ to $N_8$) visible to the receiver. The final category is related to the angular features, capturing the angle ($\theta$) formed by the line connecting the receiver to the transmitter on the horizontal plane with the positive X-axis, and the elevation angle ($\phi$) formed between the direct line connecting the transmitter and receiver and the $XY$ plane as shown in Fig. 2(a).

## III. SUPERVISED MACHINE LEARNING MODELS

In order to facilitate effective model training and evaluation, the dataset is partitioned into training and test sets, maintaining a 75:25 ratio. The training set is used to train and optimize several supervised ML models, including LR, SVR, KNN, RF, XGBoost, and DNN. The hyperparameters of these models underwent rigorous tuning for the regression problem of PL prediction. The coefficient of determination, $R^2$ score, which shows how well the data fits the regression model was used to select the hyperparameter values. $R^2$ score is calculated as follows:

$$R^2 = 1 - \frac{\sum_{j=1}^{N}(y_j - \hat{y}_j)^2}{\sum_{j=1}^{N}(y_j - \bar{y}_j)^2}; \quad \bar{y}_j = \frac{1}{N}\sum_{j=1}^{N} y_j \tag{1}$$

where $y_j$ is the actual value of the target variable and $\hat{y}_j$ is the value predicted by the model. The value of $R^2$ score closer to 1 shows a better fit. We used feature scaling to transform the input features with zero mean and unit standard deviation for an effective training process with improved convergence speed, stability, and fair consideration of all features. A coarse-to-fine grid search approach was used to find the best hyperparameters. The tuned hyperparameter values are listed in Table 3.

**TABLE 4.** Comparisons of ML model performance on the test data using various evaluation metrics.

| Models | RMSE (dB) | MAE (dB) | MAPE (%) | $R^2$ |
|---|---|---|---|---|
| LR | 5.17 | 3.72 | 3.48 | 0.45 |
| SVR | 2.53 | 1.68 | 1.59 | 0.87 |
| KNN | 2.47 | 1.48 | 1.39 | 0.87 |
| RF | **2.38** | **1.44** | **1.36** | **0.88** |
| XGBoost | 2.62 | 1.65 | 1.56 | 0.86 |
| DNN | 2.91 | 1.85 | 1.75 | 0.83 |

## IV. PERFORMANCE EVALUATION

### A. MODELS PERFORMANCE ON TEST DATASET

The trained ML models with fine-tuned hyperparameters predicted PL in the test dataset using the geometrical features as input. The performance of the ML models is validated by comparison of four matrices including mean absolute error (MAE), mean absolute percentage error (MAPE), RMSE, and coefficient of determination ($R^2$). The coefficient of determination $R^2$ has already been defined in (1). The rest of the metrics are defined as follows:

$$\text{MAE (dB)} = \frac{1}{N}\sum_{j=1}^{N}|y_j - \hat{y}_j|, \tag{2}$$

$$\text{MAPE} = \frac{1}{N}\sum_{j=1}^{N}\left|\frac{y_j - \hat{y}_j}{y_j}\right| \times 100, \tag{3}$$

$$\text{RMSE (dB)} = \sqrt{\frac{1}{N}\sum_{j=1}^{N}|y_j - \hat{y}_j|^2}, \tag{4}$$

where $y_j$ is the actual PL (dB) in the test data set, $\hat{y}_j$ is the predicted PL (dB) using one of the ML models, and $N$ is the total number of samples in the test dataset. Table 4 shows the performance comparison of ML models in PL prediction on the test dataset. Apart from the LR, all the models have almost similar performance. Notably, the RF emerges as the top-performing model across various evaluation metrics. With the lowest RMSE of 2.38 dB, the smallest MAE at 1.44 dB, a minimal MAPE of 1.36%, and $R^2$ of 0.88, RF consistently surpasses its counterparts. Random Forest achieves superior results due to its ensemble learning approach, which combines multiple decision trees to improve

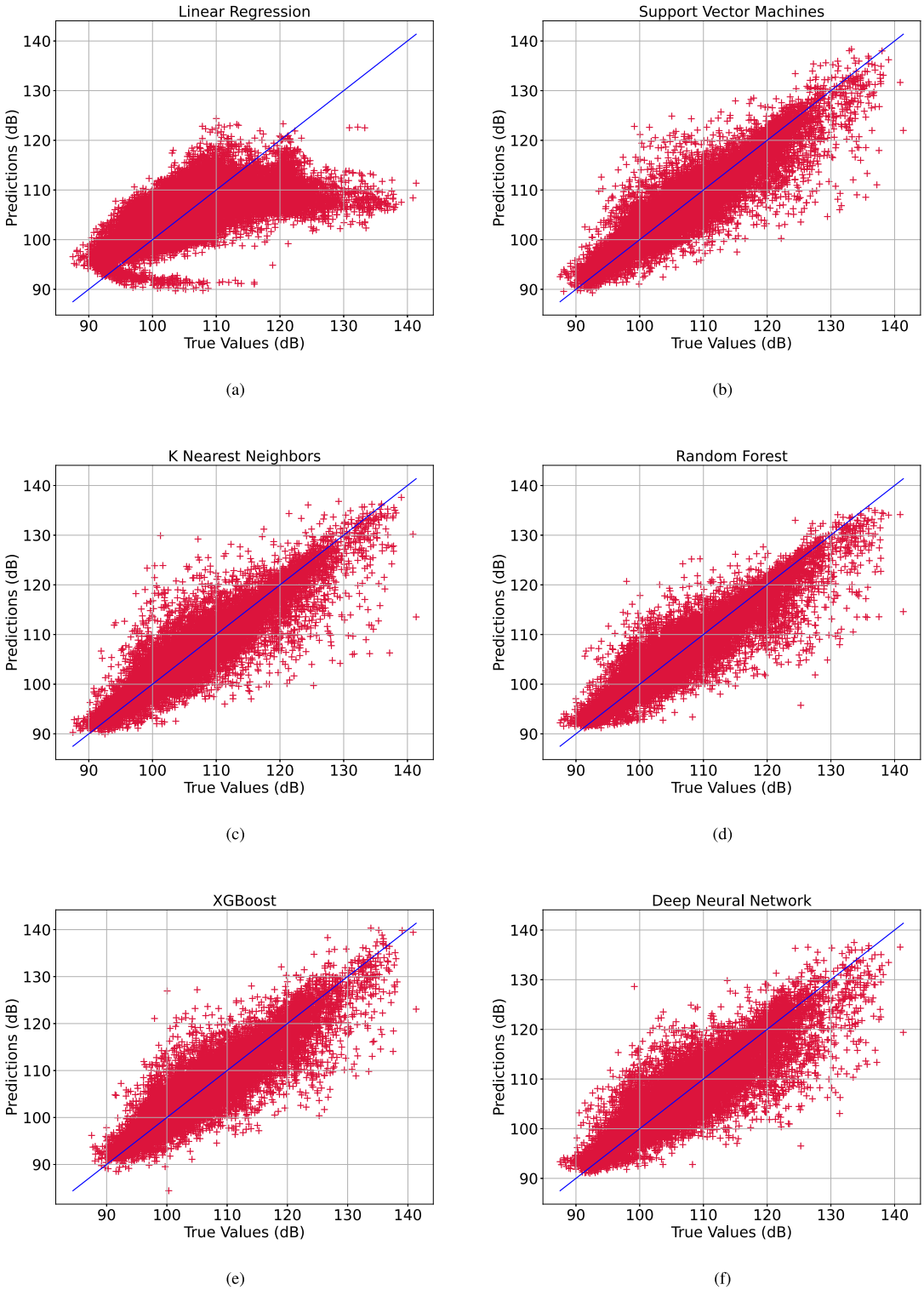


**FIGURE 3.** Path loss comparison for the test dataset: Ray-tracing versus predictions from (a) linear regression, (b) support vector machines, (c) K nearest neighbors, (d) random forest, (e) extreme gradient boosting, and (f) deep neural network.

accuracy and reduce overfitting, and its effectiveness in handling high-dimensional data by selecting random subsets of features for each split [35]. It is noteworthy that all other models, excluding LR, have demonstrated commendable performance, with an average RMSE of 2.63 dB. This advocates for the adoption of these ML models in the

design of UAV-based mmWave radio networks, presenting a computationally efficient and accurate approach with an average RMSE below 3 dB.

To provide a visual representation of the performance comparison, scatter plots depicting predicted PL values against the actual PL values for all the models are presented in Fig. 3. The scatter plots offer insightful observations on the accuracy and consistency of predictions. The LR model exhibits substantial deviations between predicted and actual values, exposing its limitations in effectively capturing the complex dependencies of PL on geometric features. In contrast, the remaining models demonstrate a more uniform and accurate alignment between predicted and actual values. The evenly distributed variations across these models signify their robust performance in capturing the non-linear relationships within the dataset.

### B. ACCURACY COMPARISON WITH EMPIRICAL MODELS

In order to evaluate the prediction accuracy of ML models against a benchmark, we evaluated the prediction error between PL computed using RT (ground truth) for Munich-1 environment against PL computed using 3GPP and ITU-R empirical models [36], [37].

PL for LOS and NLOS receivers is calculated in the 3GPP model as follows:

$$PL_{\text{LOS}} = \begin{cases} PL_1 \; 10\,\text{m} \le d_{2\text{D}} \le d'_{\text{BP}} \\ PL_2 \; d'_{\text{BP}} \le d_{2\text{D}} \le 5\,\text{km}, \end{cases} \tag{5}$$

$$\begin{aligned} PL_1 &= 32.4 + 21\log(d_{3\text{D}}) + 20\log(f_c), \\ PL_2 &= 32.4 + 40\log(d_{3\text{D}}) + 20\log(f_c) \\ &\quad - 9.5\log\Big((d'_{\text{BP}})^2 + (h_{\text{UAV}} - h_{\text{RX}})^2\Big), \\ PL_{\text{NLOS}} &= \max\big(PL_{\text{LOS}}, PL'_{\text{NLOS}}\big), \\ PL'_{\text{NLOS}} &= 13.54 + 39.08\log(d_{3\text{D}}) + 20\log(f_c) \\ &\quad - 0.6(h_{\text{RX}} - 1.5), \end{aligned} \tag{6}$$

where $d_{2\text{D}}$, $d_{3\text{D}}$, $f_c$, $h_{\text{UAV}}$, and $h_{\text{RX}}$ represent the direct 2D horizontal distance, 3D distance, carrier frequency in GHz, UAV height, and receiver height, respectively, with all distances and heights in meters. The break point distance is $d'_{\text{BP}} = 4h'_{\text{UAV}}h'_{\text{RX}}f_c/c$, where $c$ is the speed of light. Here, $h'_{\text{UAV}}$ and $h'_{\text{RX}}$ are the effective heights of the base station and receiver, calculated by subtracting $h_E = 1$ m from $h_{\text{UAV}}$ and $h_{\text{RX}}$, respectively, for urban micro-cellular environments. PL using the ITU-R model is given as follows:

$$PL(d, f) \;\; = 10\alpha\log(d) + \beta + 10\gamma\log(f_c), \quad (dB) \tag{7}$$

where, $\alpha = 2.29$, $\beta = 28.6$, and $\gamma = 1.96$ are the coefficients of the PL model. The RMSE, MAE and MAPE between PL computed using RT as ground truth and computed using 3GPP and ITU-R models are listed in Table 5. The metrics for best performing RF model are also included for comparison.

The comparison between PL prediction accuracy using empirical models and ML models reveals significant differences. 3GPP and ITU-R models show relatively higher errors with RMSE values around 7.49 dB and 7.54 dB respectively, along with MAE values of approximately 6.45 dB and 6.40 dB, and MAPE values of about 6.12% and 6.06% respectively. In contrast, ML models demonstrate superior performance, with the best performing RF model achieving an RMSE of 2.38 dB, MAE of 1.44 dB, and MAPE of 1.36%. Other ML models also exhibit competitive performance with RMSE values consistently below 3 dB, indicating better fit to the data. These results highlight the effectiveness of ML techniques in accurately predicting path loss, surpassing empirical models in accuracy and reliability.

**TABLE 5.** Comparison of PL computed using RT against empirical models.

| Models | RMSE (dB) | MAE (dB) | MAPE (%) |
|---|---|---|---|
| 3GPP | 7.49 | 6.45 | 6.12 |
| ITU-R | 7.54 | 6.40 | 6.06 |
| RF | **2.38** | **1.44** | **1.36** |

### C. MODELS PERFORMANCE ON UNSEEN URBAN ENVIRONMENTS

To evaluate the generalization capability of the proposed ML models for PL prediction in environments different from Munich-1 (Fig. 1), their performance was tested against RT simulations in five distinct urban environments. One environment is taken from Munich, and the other four are from London. These environments are labeled as Munich-2, London-1, London-2, London-3, and London-4 for future reference in this paper and are shown in Fig. 4. RT simulations were conducted for five distinct transmitter locations in each environment, each at three different altitudes: 25m, 35m, and 45m. The RT computations were performed between each transmitter location and a grid of receiver points distributed across the environments at a resolution of 5m x 5m. The number of receivers in Munich-2, London-1, London-2, London-3 and London-4 are 4735, 2895, 1771, 2445, and 1908 respectively. In this study, the receiver points within the rectangular area formed by the perimeter of buildings at the border of the environment were considered; the open area outside this perimeter was discarded. The same simulation parameters used for dataset generation in Section II-A were applied here. Geometrical features, as discussed in Section II-B, were computed for all transmitter-receiver pairs. The pre-trained ML models, trained using the dataset from Munich-1, are *directly* used to predict PL values for all transmitter locations in the new environments. The RMSE statistics including minimum value, maximum value, inter-quartile range (IQR), and median value across *all the five environments* for all the models are shown in the box plot in Fig. 5. The mean RMSE score is also shown in the plot.

The performance of the pre-trained ML models across five different environments shows notable variation in RMSE scores. Overall, the DNN model performs best on average.

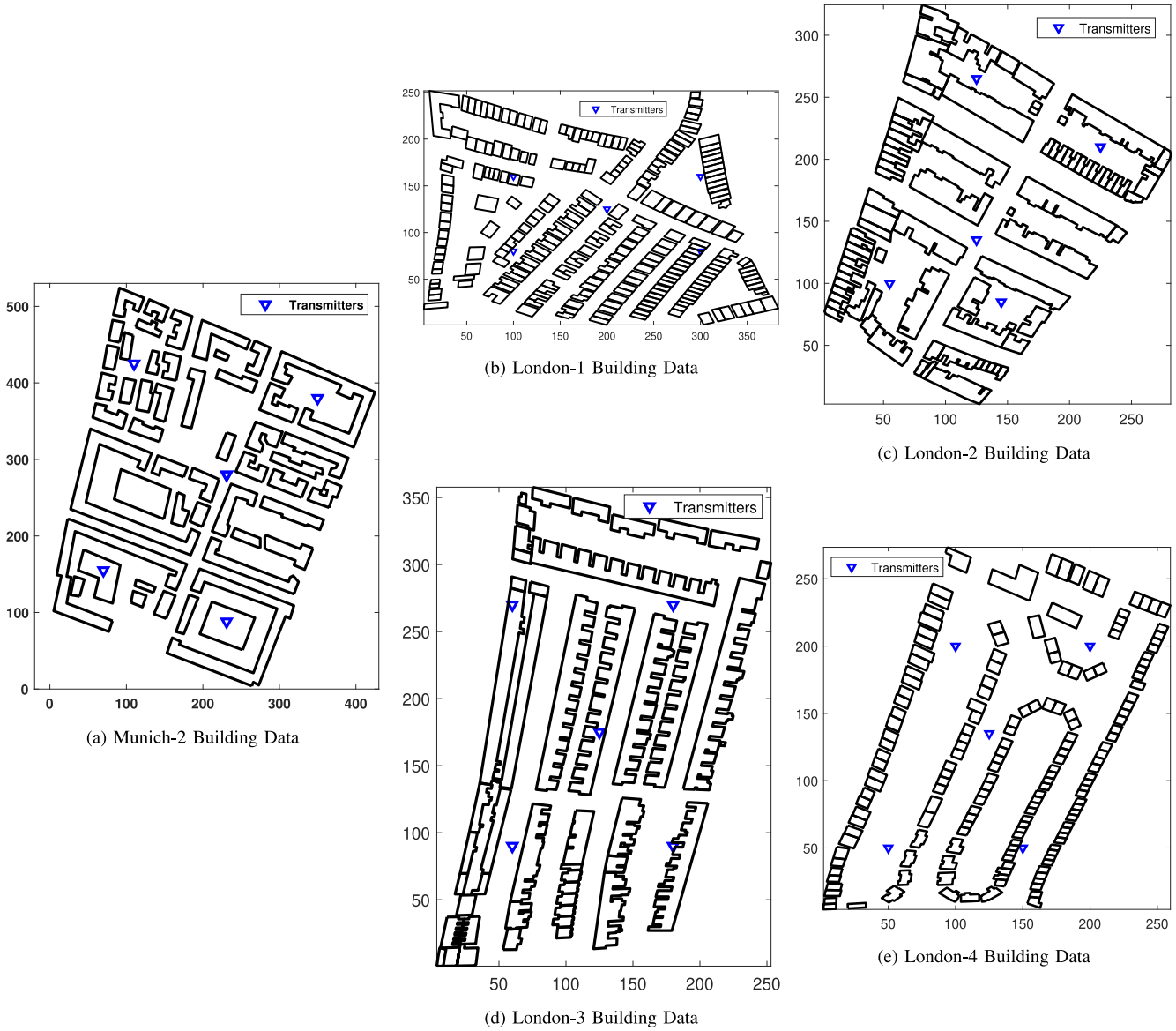


**FIGURE 4.** Building database in different locations used for validation of pre-trained models and development of models using sparse train dataset.

The mean RMSE ranges from 7.93 dB for DNN to 9.67 dB for XGBoost. The remaining models including LR, RF, KNN and SVR have the mean RMSE values of 8.09 dB, 8.41 dB, 8.61 dB, and 9.18 dB respectively. SVR demonstrated the narrowest IQR of 0.67 dB, indicating a consistent performance across different environments. Conversely, the KNN model exhibited the widest IQR of 3.38 dB, suggesting greater variability in its performance across the environments with RMSE values varying between a minimum of 5.39 dB to a maximum of 11.55 dB. LR and DNN models showed smaller variations in RMSE scores with IQR values 1.88 dB and 1.94 dB respectively. Whereas the XGBoost and RF models showed moderate variations in RMSE scores across environments with IQR scores 2.48 dB and 2.63 dB respectively.

### D. PERFORMANCE EVALUATION USING SPARSE TRAIN DATA

In the preceding section, it was clear that models trained on data from one environment struggled to generalize effectively to new environments, as indicated by significantly higher mean RMSE values compared to the best achievable values shown in the RMSE column of Table 4. This suggests that ML models must be re-trained with data specific to the new environment for optimal performance. However, the substantial data requirements for model training pose a challenge as it requires extensive RT simulations to generate large datasets. Paradoxically, this contradicts the primary aim of ML models, i.e., to provide a faster, yet accurate alternative to computationally intensive RT simulations. To address this, we explore the feasibility of training ML

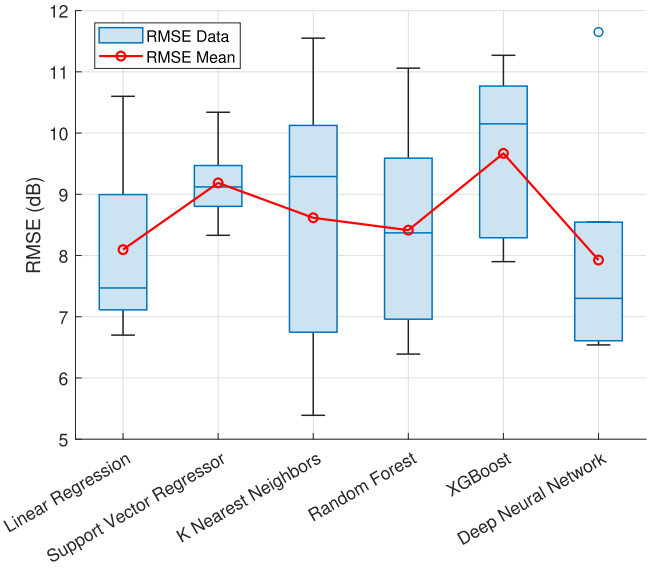


**FIGURE 5.** RMSE performance of supervised ML models on unseen urban environment.

models with *smaller, sparsely sampled datasets* derived from initial RT simulations encompassing all potential transmitter locations and heights. Utilizing the previously generated datasets in five distinct urban environments (Munich-2, London-1 to London-4) above, we evaluate how all models perform when trained on sparse data from the same urban environments. Consolidating data from all five transmitter locations in each urban environment, we trained models with varying sample sizes (5%, 10%, and 15% of the total dataset available for each environment), examining how their performance evolves. The resulting RMSE scores of supervised ML models, trained on datasets ranging from 5% to 15% sample size, are depicted in Fig. 6, alongside baseline evaluations using the conventional 75:25 train-test split ratio, providing a comprehensive comparison benchmark. It is important to note that we did not conduct extensive hyperparameter tuning during the model training phase, as was done for Munich-1. Instead, we employed a randomized search cross-validation technique to efficiently determine the optimal hyperparameters, leveraging insights gained from the previous model development cycle for Munich-1 environment (refer to Table 3).

These results highlight several key observations. When comparing these results with the generalization performance of the ML models in the previous section, it is clear that models trained on even smaller datasets (e.g., 5% sampling) from the same environment perform better than models pre-trained on larger datasets from different environment. For example, the mean RMSE for the LR model pre-trained on Munich-1 is 8.09 dB when averaged across the five environments as seen in the previous section. This value decreases to a mean RMSE of 4.26 dB (5.69 dB in Munich-2, 3.01 dB in London-1, 5.45 dB in London-2, 4.07 dB in London-3, and 3.08 dB in London-4) when the model is trained with only 5% of the dataset from the same environments. This improvement is encouraging as it indicates that prediction accuracy can be significantly enhanced by running RT computations for a small sample of receiver points across the environments and using this sparse data to train the ML models. The mean RMSE of all the models, averaged over the five environments, for each sampling is computed and shown in Fig. 6 (f).

A general trend of decreasing RMSE with increasing training dataset size is observed for all models, except for the LR model, which maintains an almost constant mean RMSE of 4.2 dB across all samplings. The ensemble learning models, RF and XGBoost, consistently perform best across the environments for all samplings, achieving a mean RMSE as low as 3.5 dB with a 15% training dataset size. Interestingly, the DNN struggles with lower sample sizes and performs poorly, with mean RMSEs of 5.34 dB, 4.55 dB, and 4 dB for 5%, 10%, 15% sampling, respectively. This aligns with the fact that DNN models require large amounts of data for better accuracy. SVR and KNN models perform slightly better than LR and DNN, with mean RMSE values below 4 dB for SVR and around 4 dB for KNN for small sampling sizes between 5% and 15%. The variability in models performances in different urban environments is also observed. Models achieved lowest RMSE values in London-4, whereas Munich-2 proved to be the most challenging, with highest RMSE values observed for all models across all samplings. It is noteworthy that the baseline models utilizing a 75:25 train-test split do not achieve the same level of performance as observed in Section IV-A for Munich-1, where a very large training dataset was utilized and an extensive hyperparameters tuning was performed.

To evaluate the computational performance gains from using sparsely sampled training datasets, let $t_F$ denote the time required for computing geometrical features, and $t_\Delta$ denote the time for RT computations for a given sampling rate (5% to 15%). The total time required for PL estimation using the ML model, $t_{ML}$, is

$$t_{ML} = t_F + t_\Delta. \tag{8}$$

Note that the ML model training and inference times are excluded from these calculations as they are negligible compared to $t_F$ and $t_\Delta$. This holds true for all models except SVR, which requires significant training time for larger datasets. Considering $t_{RT}$ represents the total time required for PL computation using RT for the complete environment, the percentage reduction ($R$) in computation time using the ML model compared to RT can be calculated as follows:

$$R\% = \left(\frac{t_{RT} - t_{ML}}{t_{RT}}\right) \times 100. \tag{9}$$

Table 6 illustrates the computational performance comparison across different sampling rates (5%, 10%, and 15%) for the five urban environments. The time required for computing geometrical features ($t_F$) and ray tracing ($t_{RT}$) are presented for each environment. All the times are in

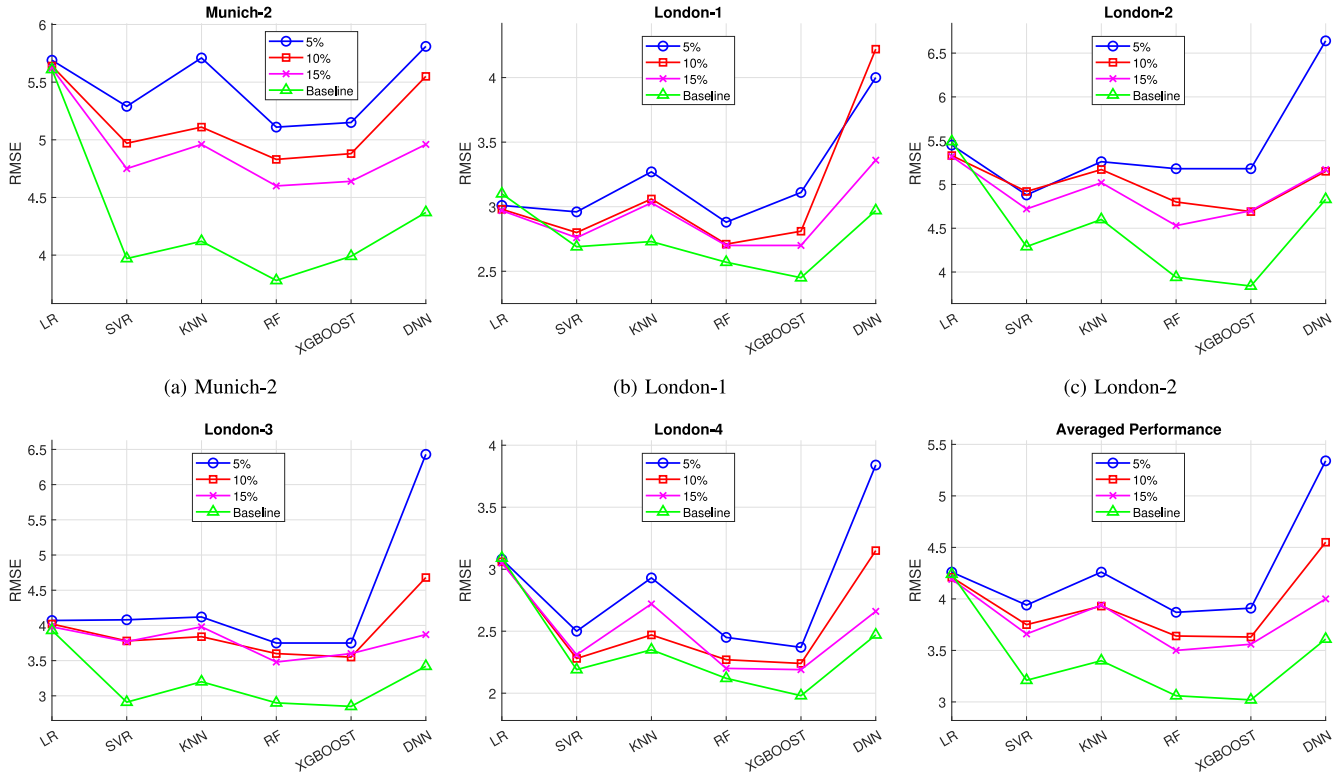


(a) Munich-2 (b) London-1 (c) London-2

(d) London-3 (e) London-4 (f) Average RMSE Performance

**FIGURE 6.** Machine learning models performance on sparse train data in different urban environments.

**TABLE 6.** Computational performance comparison for different sampling rates.

| Sampling Rate | Munich-2 | | London-1 | | London-2 | | London-3 | | London-4 | |
|---|---|---|---|---|---|---|---|---|---|---|
| | $t_F$ | $t_{RT}$ | $t_F$ | $t_{RT}$ | $t_F$ | $t_{RT}$ | $t_F$ | $t_{RT}$ | $t_F$ | $t_{RT}$ |
| | 18706 | 22424 | 13408 | 15290 | 6127 | 7352 | 6197 | 8271 | 9877 | 11690 |
| | $t_\Delta$ | $R$ | $t_\Delta$ | $R$ | $t_\Delta$ | $R$ | $t_\Delta$ | $R$ | $t_\Delta$ | $R$ |
| 5% sampling | 1087 | 11.73 | 742 | 7.46 | 357 | 11.87 | 401 | 20.22 | 567 | 10.66 |
| 10% sampling | 2287 | 6.38 | 1560 | 2.11 | 750 | 6.46 | 843 | 14.87 | 1192 | 5.31 |
| 15% sampling | 3498 | 0.98 | 2316 | -2.84 | 1114 | 1.51 | 1290 | 9.47 | 1771 | 0.36 |

seconds. An Intel Core i7 computer with 16 GB RAM is used in simulations. The results show a significant reduction in computation time using the ML model compared to RT. For instance, at a 5% sampling rate, the time reduction $R$ in London-3 is the highest at 20.22%, while Munich-2 also shows a notable reduction of 11.73%. However, the gains decrease with increased sampling rates. This indicates that the time gains will decrease as more data is used to train the ML models for better accuracy. A negative time reduction of -2.84% is recorded at 15% sampling for London-1 which indicates that it takes more time for ML model than simply running complete RT for London-1. These results highlights the efficiency of using ML models with lower sampling rates to achieve substantial time savings in PL estimation with moderate accuracy.

The above analysis implies that the RF model can be trained on a sparse dataset to achieve computationally efficient and reasonably accurate PL prediction in any given urban environment. Algorithm 1 outlines the necessary steps for predicting PL in an urban environment.

### *E. MODELS PERFORMANCE WITH NOISY INPUT FEATURES*

To assess the impact of estimation error in input geometrical features on ML model performance, the models were trained on the same training dataset generated for Munich-1. Prior to evaluation on the test dataset, uniform random noise was introduced to the input features of the test dataset, with noise levels ranging from 5% to 15% of the feature values. The models' performance was then evaluated. Fig. 7 illustrates

**Algorithm 1** Path Loss Prediction Using Sparse Train Data

**Require:** Buildings vector data, transmitter locations, receiver grid, carrier frequency, and sampling rate (5% to 15%) for train data.

**Ensure:** Radio coverage map for all transmitter locations

```
Initialize empty matrix P
for each transmitter location t do
    for each receiver location r do
        Add (t, r) to P
    end for
end for
Initialize empty features matrix G
for each (t, r) pair in P do
    Compute features F for transmitter t and receiver r
    Add F to G
end for
Randomly sample a fraction of transmitter-receiver pairs at the specified sampling rate from P
Extract corresponding feature subsets from G for sample points
Compute PL using RT simulations for sample points
Train a Random Forest model M using the sampled data:
    Input: Sampled transmitter-receiver pairs and corresponding features and path loss
    Output: Trained Random Forest model M
Use M to compute path loss estimates for the remaining transmitter-receiver pairs
return Estimated radio coverage map for all transmitter locations
```

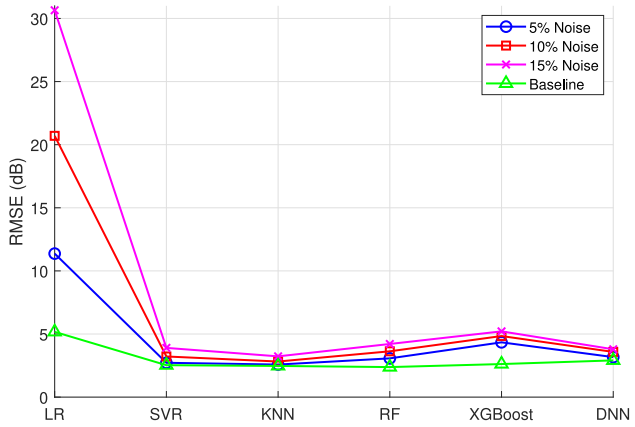


**FIGURE 7.** Performance comparison with noisy input features.

the RMSE of the ML models at various noise thresholds, with the RMSE of all models on the noise-free data (Table 4) also plotted as a baseline.

The analysis of RMSE performance for ML models with noisy input features shows that Linear Regression (LR) is highly sensitive to noise, with RMSE increasing significantly from 11.37 dB to 20.7 dB to 30.65 dB as noise levels rise from 5% to 10% to 15%. In contrast, the other models

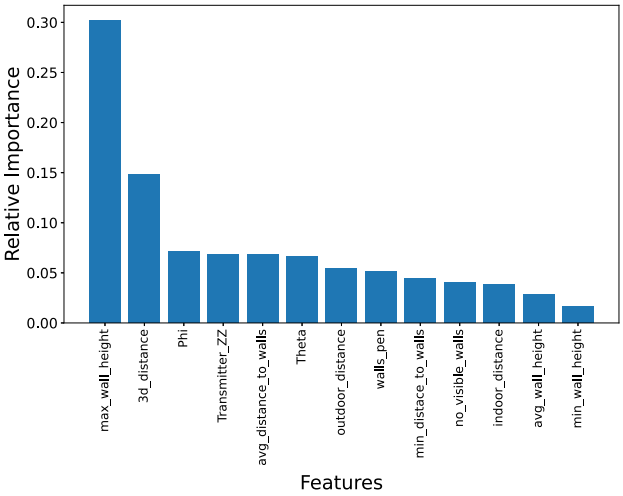


**FIGURE 8.** Relative importance of features in Random Forest model.

demonstrate robustness, with relatively smaller increases in RMSE under noise conditions. Interestingly, KNN performs better than RF with noisy input features, as evidenced by its lower RMSE values under all noise conditions.

### F. FEATURE IMPORTANCE AND SEQUENTIAL FEATURE INCLUSION

The above results highlight the RF model's remarkable ability to predict PL with a minimal RMSE. To gain insights into the model's decision-making process, a feature importance analysis is conducted using the Scikit Learn API. The results, depicted in Fig. 8, present the relative importance of geometrical features in descending order for the RF model that gives the best RMSE score of 2.38 dB on the test dataset (see Table 4). Notably, the feature corresponding to the maximum height of the buildings obstructing the receiver holds the highest relative importance of 0.3. This is followed by the 3D distance between the transmitter and receiver, with a relative importance of 0.15. Subsequently, the angular parameters ($\phi$ and $\theta$), transmitter height, and the average distance between the receiver and visible walls exhibit relative importance ranging from 0.07 to 0.066. The remaining input features demonstrate progressively lower relative importance, as illustrated in the figure.

To further investigate the model's performance with varying sets of input features, a sequential feature inclusion approach is used. Initially, the RF model is trained using only the single feature with the highest feature importance value, and its RMSE is assessed on the test dataset. We used the larger dataset for train and test as discussed in Section II. Subsequently, the model undergoes additional training phases, each time incorporating the feature with the next highest importance value. This sequential process is iterated until all feature combinations are exhaustively tested. Fig. 9 illustrates the RMSE values evaluated on the test dataset as the number of features is sequentially increased during model training. The RMSE on the test dataset varies

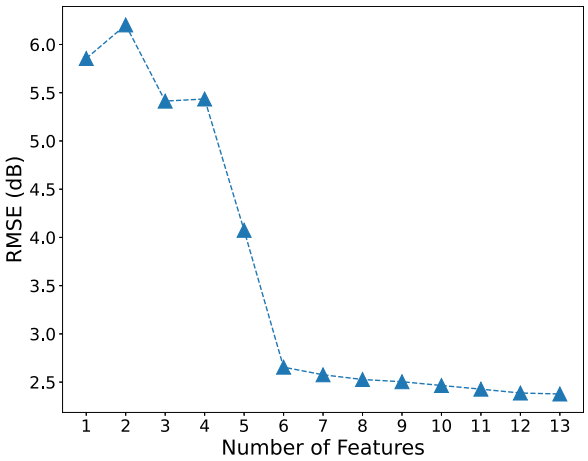


**FIGURE 9.** Comparison of Model's performance with increasing number of features.

from 5.85 dB to 4.07 dB for combinations involving the top 4 features, with the highest RMSE of 6.2 dB observed for top 2 features. A notable decrease in RMSE is then observed, sharply declining to 2.65 dB for the combination of 6 features. Following this, the RMSE demonstrated a minor and consistent decrease, reaching 2.38 dB for the remaining 7 features used in the training. This also implies that the RF model can be trained using only the six features without significantly affecting the RMSE score.

## V. CONCLUSION

This paper investigated the performance of classical supervised ML models in predicting PL in urban UAV-assisted mmWave radio networks, leveraging a unique set of thirteen geometrical features. The findings showed the superior performance of the RF model, surpassing all counterparts across multiple evaluation metrics, with an RMSE of 2.38 dB, MAE of 1.44 dB, MAPE of 1.36%, and an impressive $R^2$ score of 0.88. The proposed ML models demonstrate better accuracy than 3GPP and ITU models. The models, however, exhibited limited generalization capability to unseen environments, and require re-training with data specific to the new environment. To address this limitation, we extensively evaluated the accuracy improvements and reductions in run times when the models were trained using sparse data across five different urban environments. An analysis of the sensitivity of ML models to noisy input geometrical features revealed that the LR model exhibited the largest variations in accuracy with noisy inputs. Additionally, an analysis of the importance of geometrical features showed that the RF model could still achieve a commendable RMSE of 2.65 dB with only six features, emphasizing its robustness.

## REFERENCES

[1] M. Noor-A-Rahim et al., "6G for vehicle-to-everything (V2X) communications: Enabling technologies, challenges, and opportunities," *Proc. IEEE*, vol. 110, no. 6, pp. 712–734, Jun. 2022.

[2] G. Geraci et al., "What will the future of UAV cellular communications be? A flight from 5G to 6G," *IEEE Commun. Surveys Tuts.*, vol. 24, no. 3, pp. 1304–1335, 3rd Quart., 2022.

[3] A. Al-Hourani, S. Kandeepan, and S. Lardner, "Optimal LAP altitude for maximum coverage," *IEEE Wireless Commun. Lett.*, vol. 3, no. 6, pp. 569–572, Dec. 2014.

[4] H. Wang, H. Zhao, W. Wu, J. Xiong, D. Ma, and J. Wei, "Deployment algorithms of flying base stations: 5G and beyond with UAVs," *IEEE Internet Things J.*, vol. 6, no. 6, pp. 10009–10027, Dec. 2019.

[5] X. Cheng and Y. Li, "A 3-D geometry-based stochastic model for UAV-MIMO wideband nonstationary channels," *IEEE Internet Things J.*, vol. 6, no. 2, pp. 1654–1662, Apr. 2019.

[6] I. Mohammed, S. Gopalam, I. B. Collings, and S. V. Hanly, "Closed form approximations for UAV line-of-sight probability in urban environments," *IEEE Access*, vol. 11, pp. 40162–40174, 2023.

[7] A. Saboor, E. Vinogradov, Z. Cui, A. Al-Hourani, and S. Pollin, "A geometry-based modelling approach for the line-of-sight probability in UAV communications," *IEEE Open J. Commun. Soc.*, vol. 5, pp. 364–378, 2024.

[8] S. H. Alsamhi, F. A. Almalki, O. Ma, M. S. Ansari, and B. Lee, "Predictive estimation of optimal signal strength from drones over IoT frameworks in smart cities," *IEEE Trans. Mobile Comput.*, vol. 22, no. 1, pp. 402–416, Jan. 2023.

[9] M. Akbari, A. Syed, W. S. Kennedy, and M. Erol-Kantarci, "Constrained federated learning for AoI-limited SFC in UAV-aided MEC for smart agriculture," *IEEE Trans. Mach. Learn. Commun. Netw.*, vol. 1, pp. 277–295, Sep. 2023.

[10] S. Shakoor, Z. Kaleem, M. I. Baig, O. Chughtai, T. Q. Duong, and L. D. Nguyen, "Role of UAVs in public safety communications: Energy efficiency perspective," *IEEE Access*, vol. 7, pp. 140665–140679, 2019.

[11] X. Tang, F. Chen, F. Wang, and Z. Jia, "Disaster-resilient emergency communication with intelligent air–ground cooperation," *IEEE Internet Things J.*, vol. 11, no. 3, pp. 5331–5346, Feb. 2024.

[12] D. K. Jain, Y. Li, M. J. Er, Q. Xin, D. Gupta, and K. Shankar, "Enabling unmanned aerial vehicle borne secure communication with classification framework for industry 5.0," *IEEE Trans. Ind. Informat.*, vol. 18, no. 8, pp. 5477–5484, Aug. 2022.

[13] P. Dong, X. Wang, S. Wang, Y. Wang, Z. Ning, and M. S. Obaidat, "Internet of UAVs based remote health monitoring: An online eHealth system," *IEEE Wireless Commun.*, vol. 28, no. 3, pp. 15–21, Jun. 2021.

[14] L. D. Nguyen, A. Kortun, and T. Q. Duong, "An introduction of real-time embedded Optimisation programming for UAV systems under disaster communication," *EAI Endorsed Trans. Ind. Netw. Intell. Syst.*, vol. 5, no. 17, p. e5, Dec. 2018.

[15] "UAV market by point of sale." MandM. Accessed: May 1, 2024. [Online]. Available: https://www.marketsandmarkets.com/Market-Reports/unmanned-aerial-vehicles-uav-market-662.html

[16] M. Elkashlan, T. Q. Duong, and H.-h. Chen, "Millimeter-wave communications for 5G–part-2: Applications [guest editorial]," *IEEE Commun. Mag.*, vol. 53, no. 1, pp. 166–167, Jan. 2015.

[17] *Propagation Data and Prediction Methods Required for the Design of Terrestrial Broadband Radio Access Systems Operating in a Frequency Range from 3 GHz to 60 GHz*, ITU-Rec. P. 1410, Int. Telecommun. Union, Geneva, Switzerland, Accessed: Jul. 22, 2024. [Online]. Available: https://www.itu.int/rec/R-REC-P.1410-6-202308-I/en

[18] S. J. Maeng, H. Kwon, O. Ozdemir, and I. Guvenc, "Impact of 3-D antenna radiation pattern in UAV air-to-ground path loss modeling and RSRP-based localization in rural area," *IEEE Open J. Antennas Propagat.*, vol. 4, pp. 1029–1043, 2023.

[19] M. Song, Y. Huo, Z. Liang, X. Dong, and T. Lu, "Air-to-ground large-scale channel characterization by ray tracing," *IEEE Access*, vol. 10, pp. 125930–125941, 2022.

[20] X. Cheng, Y. Li, C.-X. Wang, X. Yin, and D. W. Matolak, "A 3-D geometry-based stochastic model for unmanned aerial vehicle MIMO Ricean fading channels," *IEEE Internet Things J.*, vol. 7, no. 9, pp. 8674–8687, Sep. 2020.

[21] H. Li et al., "Air-to-ground path loss prediction using ray tracing and measurement data jointly driven DNN," *Comput. Commun.*, vol. 196, pp. 268–276, Dec. 2022.

[22] K. Mao et al., "ML-based delay–angle-joint path loss prediction for UAV mmWave channels," *Wireless Netw.*, vol. 30, pp. 3947–3959, Oct. 2021.

[23] H. Zhang, J. Dong, X. Liu, J. Liu, and X. Zhang, "An artificial intelligence radio propagation model based on geographical information," *IEEE Trans. Antennas Propag.*, vol. 70, no. 12, pp. 12049–12060, Dec. 2022.

[24] G. Yang, Y. Zhang, Z. He, J. Wen, Z. Ji, and Y. Li, "Machine-learning-based prediction methods for path loss and delay spread in air-to-ground millimetre-wave channels," *Inst. Eng. Technol. Microw., Antennas Propagat.*, vol. 13, no. 8, pp. 1113–1121, Apr. 2019.
[25] U. Masood, H. Farooq, A. Imran, and A. Abu-Dayya, "Interpretable AI-based large-scale 3D Pathloss prediction model for enabling emerging self-driving networks," *IEEE Trans. Mobile Comput.*, vol. 22, no. 7, pp. 3967–3984, Jul. 2023.
[26] S. P. Sotiroudis, G. Athanasiadou, G. Tsoulos, P. Sarigiannidis, C. G. Christodoulou, and S. K. Goudos, "Evolutionary ensemble learning pathloss prediction for 4G and 5G flying base stations with UAVs," *IEEE Trans. Antennas Propag.*, vol. 71, no. 7, pp. 5994–6005, Jul. 2023.
[27] S. P. Sotiroudis, A. D. Boursianis, S. K. Goudos, and K. Siakavara, "From spatial urban site data to path loss prediction: An ensemble learning approach," *IEEE Trans. Antennas Propag.*, vol. 70, no. 7, pp. 6101–6105, Jul. 2022.
[28] S. P. Sotiroudis, G. Athanasiadou, G. V. Tsoulos, C. Christodoulou, and S. K. Goudos, "Ensemble learning for 5G flying base station path loss modelling," in *Proc. 16th Eur. Conf. Antennas Propag. (EuCAP)*, 2022, pp. 1–4.
[29] S. K. Goudos and G. Athanasiadou, "Application of an ensemble method to UAV power modeling for cellular communications," *IEEE Antennas Wireless Propag. Lett.*, vol. 18, pp. 2340–2344, 2019.
[30] S. C. Lam and X. N. Tran, "Improving performance of the typical user in the indoor cooperative NOMA Millimeter wave networks with presence of walls," *EAI Endorsed Trans. Ind. Netw. Intell. Syst.*, vol. 11, no. 2, p. e4, Apr. 2024.
[31] S. Hussain and C. Brennan, "Efficient preprocessed ray tracing for 5G mobile transmitter scenarios in urban microcellular environments," *IEEE Trans. Antennas Propag.*, vol. 67, no. 5, pp. 3323–3333, May 2019.
[32] S. Hussain and C. Brennan, "A dynamic visibility algorithm for ray tracing in outdoor environments with moving transmitters and scatterers," in *Proc. 14th Eur. Conf. Antennas Propag. (EuCAP)*, 2020, pp. 1–5.
[33] S. Hussain and C. Brennan, "A visibility matching technique for efficient Millimeter-wave vehicular channel modeling," *IEEE Trans. Antennas Propag.*, vol. 70, no. 10, pp. 9977–9982, Oct. 2022.
[34] V. Degli-Esposti, F. Fuschini, E. M. Vitucci, and G. Falciasecca, "Measurement and modelling of scattering from buildings," *IEEE Trans. Antennas Propag.*, vol. 55, no. 1, pp. 143–153, Jan. 2007.
[35] L. Breiman, "Random forests," *Mach. Learn.*, vol. 45, no. 1, pp. 5–32, Oct. 2001.
[36] *Propagation Data and Prediction Methods for the Planning of Short-Range Outdoor Radiocommunication Systems and Radio Local Area Networks in the Frequency Range 300 MHz to 100 GHz*, ITU-Rec. P. 1411, Accessed: Jul. 22, 2024. [Online]. Available: https://www.itu.int/rec/R-REC-P.1411/en
[37] "Study on channel model for frequency spectrum above 6 GHz; (Release 14), Version 14.2.0," 3GPP, Sophia Antipolis, France, Rep. TR 38.900, Accessed: Jul. 22, 2024. [Online]. Available: https://portal.3gpp.org/

**SAJJAD HUSSAIN** received the B.Sc. degree in electrical engineering from the University of Engineering and Technology at Taxila, Taxila, Pakistan, in 2006, the M.Sc. degree in telecommunications engineering from the University of Liverpool, Liverpool, U.K., in 2008, and the Ph.D. degree in electronic engineering from Dublin City University, Dublin, Ireland, in 2017. From 2009 to 2013, he was a Technical and Test Engineer with Vodafone Automotive Ltd., Manchester, U.K. He is currently an Assistant Professor with the School of Electrical Engineering and Computer Sciences, National University of Sciences and Technology, Islamabad, Pakistan. His research interests include radio channel modeling for future radio networks using ray tracing and machine learning.

**SYED FARAZ NAEEM BACHA** received the B.Sc. degree in electrical engineering from the University of Engineering and Technology at Peshawar, Peshawar, Pakistan, in 2019, and the M.Sc. degree in electrical engineering from the School of Electrical Engineering and Computer Science, National University of Sciences and Technology, Islamabad, Pakistan, in 2023. His research interests include radio channel modeling in UAV-assisted mmwave radio networks.

**ADNAN AHMAD CHEEMA** (Member, IEEE) received the B.Sc. degree from COMSATS University, Pakistan, in 2006, the M.Sc. degree from the King's College London, U.K., in 2008, and the Ph.D. degree from the Durham University, U.K., in 2015. From 2015 to 2017, he was a Postdoctoral Research Associate with Durham University and was involved in 5G channel measurements and modeling (sub-6 GHz and 24-90 GHz). In 2017, he joined Ulster University, U.K., as a Lecturer of Electronics Engineering. His research interests include wireless communications, channel modeling, reconfigurable intelligent surface, nonorthogonal multiple access, and machine learning.

**BERK CANBERK** (Senior Member, IEEE) has been an Adjunct Professor with the Department of Electrical and Computer Engineering, Northeastern University since 2016. He is currently a Professor with Edinburgh Napier University, U.K., and is also with the Department Artificial Intelligence and Data Engineering, Istanbul Technical University. His current research interests include AI driven network automation and management, software-defined networking, 5G, 6G, and intelligent aerial networks. He was a recipient of the IEEE INFOCOM Best Poster Paper Award in 2015, the IEEE CAMAD Best Paper Award in 2016, the British Council (U.K.) Researcher Link Award in 2017, the IEEE Turkey Research Incentive Award in 2018, and the IEEE INFOCOM Best Paper Award in 2018.

**TRUNG Q. DUONG** (Fellow, IEEE) is a Canada Excellence Research Chair and a Full Professor with the Memorial University of Newfoundland, Canada. He is also the Adjunct Chair Professor of Telecommunications with Queen's University Belfast, U.K. His current research interests include quantum communications, wireless communications, signal processing, machine learning, and realtime optimization.

Dr. Duong received the Best Paper Award at the IEEE VTC-Spring 2013, IEEE ICC 2014, IEEE GLOBECOM 2016, 2019, and 2022, IEEE DSP 2017, IWCMC 2019 and 2023, and IEEE CAMAD 2023. He has received the two prestigious awards, including the Research Chair of the Royal Academy of Engineering from 2021 to 2025 and the Royal Academy of Engineering Research Fellowship from 2015 to 2020. He is the recipient of the prestigious Newton Prize in 2017. He has served as an Editor/Guest Editor for the IEEE TRANSACTIONS ON WIRELESS COMMUNICATIONS, IEEE TRANSACTIONS ON COMMUNICATIONS, IEEE TRANSACTIONS ON VEHICULAR TECHNOLOGY, IEEE COMMUNICATIONS LETTERS, IEEE WIRELESS COMMUNICATIONS LETTERS, IEEE WIRELESS COMMUNICATIONS, IEEE COMMUNICATIONS MAGAZINES, and IEEE JOURNAL ON SELECTED AREAS IN COMMUNICATIONS.